

Transworld Research Network
37/661 (2), Fort P.O., Trivandrum-695 023, Kerala, India



Recent Res. Devel. Fluid Dynamics, 4(2003): 159-179 ISBN: 81-7895-101-0

9

Slender vortex motion

Hongyun Wang and Hong Zhou

Department of Applied Mathematics and Statistics, University of California
Santa Cruz, CA 95064

Abstract

A fast numerical method based on the Klein-Knio's thin filament model is presented for computing the motion of slender vortex filaments. Combining the Biot-Savart law and an asymptotic expansion, Klein and Knio derived an equation for the evolution of a thin vortex filament. However, in their numerical discretization the spatial step is restricted by the overlapping condition of the traditional thin tube method. That is, the spatial step has to be small in comparison with the core of the vortex filament. The stiffness of the system is inversely proportional to the square of the spatial step. As a result, a small spatial step requires a tiny time step, thereby makes the simulations virtually impossible for thin filaments. Here we propose a fast numerical method to overcome this difficulty. In our approach, the spatial discretization does not depend on the core size. Our method significantly speeds up the computation for thin vortex filament.

Correspondence/Reprint request: Dr. Hong Zhou, Department of Applied Mathematics and Statistics, University of California Santa Cruz, CA 95064. E-mail : hongzhou@ams.ucsc.edu

1. Introduction

Thin vortex filament model has an important application in the prediction of the behavior of the trailing vortices behind aircraft (Crow [1], Ting [2], Widnall [3]). Chorin [4] and Chorin and Akaio [5] suggest that slender vortices play an important role in governing the structure of turbulent flows. In addition, superfluid vortex filaments are observed to be smooth and have very tiny core radius ($\sim 1\text{\AA}$) [6]. So the thin filament model fits perfectly with the superfluid vortex filaments. These are just a few of the ample motivations for the studies of thin vortex filament dynamics.

The irrotational flow surrounding a three-dimensional concentrated slender vortex is described by the well-known Biot-Savart law

$$\mathbf{v}(\mathbf{x}) = -\frac{\Gamma}{4\pi} \int_C \frac{\mathbf{x} - \mathbf{x}'}{|\mathbf{x} - \mathbf{x}'|^3} \times d\mathbf{x}', \quad (1)$$

where C is the vortex centerline. This induced velocity field becomes singular as one approaches points on C . There are many approximations based on (1) to model slender vortex flow, including the self-induction approximation [7], the Klein-Majda equation [8], and vortex-element-based thin-tube method [9]. All these approaches simplify vortex core dynamics by either ignoring core structure or assuming a constant core. Klein and Knio [10] presented a thin filament model, which was originated from Callegari and Ting [11]. In this model, the core vorticity distribution is assumed to evolve slowly compared to the core rotation rate. In [10] they also developed a numerical scheme for the simulation of slender vortex filaments. The advantage of their approach is that the core structure evolution is included. However, their numerical scheme based on the vortex-element method is restricted by the overlapping condition, which could be very expensive and inefficient for thin vortex motion. In this paper, we develop a fast numerical method for Klein and Knio's thin filament model. Our method no longer requires the overlapping condition, thereby significantly speeds up the numerical simulations. Our numerical method can be easily extended to solve the Klein-Knio-Ting model [12] for viscous slender vortices.

The paper is organized as follows. We start with an introduction to the thin filament model, followed by a brief review of Klein and Knio's numerical method. Then we give a detailed description of our fast method. Numerical experiments are carried out for superfluid vortex motion.

2. Thin filament model

A thin vortex filament is a vorticity distribution that is highly concentrated in the vicinity of a smooth time-dependent curve $L(t) : s \rightarrow \mathbf{x}(s, t)$ as sketched in Fig. 1. The radius δ of the vortex core is much smaller than a characteristic radius of curvature R of $L(t)$. $L(t)$ is usually called the centerline of the filament. However, this is not a very good definition for the centerline. According to this definition, any smooth curve $\tilde{L}(t)$ within $O(\delta^2)$ range of $L(t)$ is also a centerline. More important, $L(t)$ may not be a material trajectory of $\mathbf{x}(s, 0)$, i.e., $L(t)$ may not move with the fluid. Even if $L(t)$ moves with the fluid, the vorticity distribution observed relative to $L(t)$ and the motion of $L(t)$ may be changing very rapidly. As we will see below, if we follow an arbitrary centerline

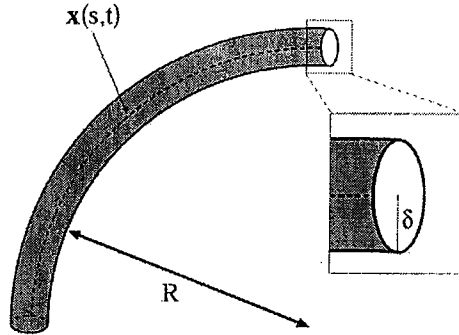


Figure 1. Sketch of a thin vortex filament.

$L(t)$, the characteristic time for the vorticity distribution relative to $L(t)$ is $t_{core} \sim \frac{\delta^2}{\Gamma}$, where Γ is the circulation of the vortex filament. Thus as the core radius δ becomes smaller and smaller, it is impossible to get an asymptotic equation for an arbitrary centerline $L(t)$. To derive an asymptotic equation, the following model (called the thin filament model) was studied by Klein and Knio [10].

Let $L(t) : s \rightarrow \mathbf{x}(s, t)$ be the trajectory of a special curve $\mathbf{x}(s, 0)$ and let (r, θ, s) be the curve attached coordinate system as shown in Fig. 2. We assume that the curve $\mathbf{x}(s, t)$ has the following properties:

(a) Vorticity distribution observed relative to $\mathbf{x}(s, t)$ has the asymptotic expansion form

$$\begin{aligned} \omega(\mathbf{x}, t; \delta) &= \frac{1}{\delta^2} \left[\eta^{(0)}\left(\frac{r}{\delta}, s, t\right) \mathbf{e}_\theta + \zeta^{(0)}\left(\frac{r}{\delta}, s, t\right) \mathbf{e}_r \right] \\ &+ \frac{1}{\delta} \left[\xi^{(1)}\left(\frac{r}{\delta}, \theta, s, t\right) \mathbf{e}_r + \eta^{(1)}\left(\frac{r}{\delta}, \theta, s, t\right) \mathbf{e}_\theta + \zeta^{(1)}\left(\frac{r}{\delta}, \theta, s, t\right) \mathbf{e}_t \right] \\ &+ O(1); \end{aligned} \quad (2)$$

(b) Vorticity distribution observed relative to $\mathbf{x}(s, t)$ is quasi-steady. More specifically, in a mathematical language, that means

$$\frac{\partial}{\partial t} \eta^{(0)}, \frac{\partial}{\partial t} \zeta^{(0)}, \frac{\partial}{\partial t} \xi^{(1)}, \frac{\partial}{\partial t} \eta^{(1)}, \frac{\partial}{\partial t} \zeta^{(1)} \sim O\left(\frac{\Gamma^2}{R^2}\right). \quad (3)$$

Note that assumption (b) implies that the characteristic time of the core structure evolution relative to $\mathbf{x}(s, t)$ is

$$t_{ref} \sim \frac{R^2}{\Gamma}, \quad (4)$$

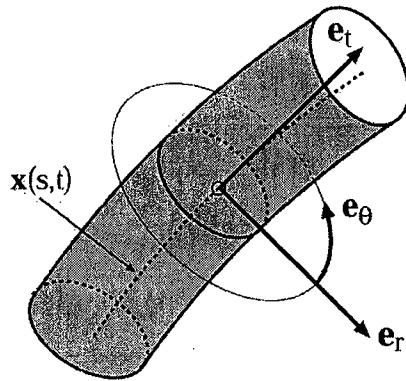


Figure 2. A curve attached coordinate system.

whereas the characteristic turn-over time of the vortex core is much smaller

$$t_{core} \sim \frac{\delta^2}{\Gamma}. \quad (5)$$

That is why we use the word “quasi-steady”: The rate of the change of the vorticity distribution relative to $\mathbf{x}(s, t)$ is much smaller than that of the rotation of the vortex core. The curve $\mathbf{x}(s, t)$ satisfying assumptions (a) and (b) is called *the line of stagnation points*. A stagnation point is a point such that if we move with it, we will see a quasi-steady core structure. It is uniquely defined. Through the following example, one can see that the vorticity distribution is quasi-steady only if it is observed from the line of stagnation points. Consider a straight vortex filament along the z -axis with vorticity distribution

$$\omega(x, y, z) = \frac{1}{\delta^2} e^{-(x^2+y^2)/\delta^2} \mathbf{e}_z, \quad (6)$$

where \mathbf{e}_z is the unit vector in z direction.

If we stand at the origin $(0, 0, 0)$, we see a steady vorticity distribution:

$$\omega\left(\frac{r}{\delta}, \theta, s, t\right) = \frac{1}{\delta^2} e^{-r^2/\delta^2} \mathbf{e}_z. \quad (7)$$

Suppose that we select $(\alpha, 0, 0)$ at time $= 0$ as the observation point ($\alpha \sim \delta^2$). At time $= t$, the Cartesian coordinates of the observation point are $(\alpha \cos(\beta t), \alpha \sin(\beta t), 0)$ where $\beta \sim \frac{1}{\delta^2}$ is the angular velocity. Let us follow the evolution of vorticity at the point that has polar coordinates (r, θ) relative to the observation point $(\alpha \cos(\beta t), \alpha \sin(\beta t))$. The Cartesian coordinates of this point are denoted by $(x(t), y(t))$ (Fig. 3).

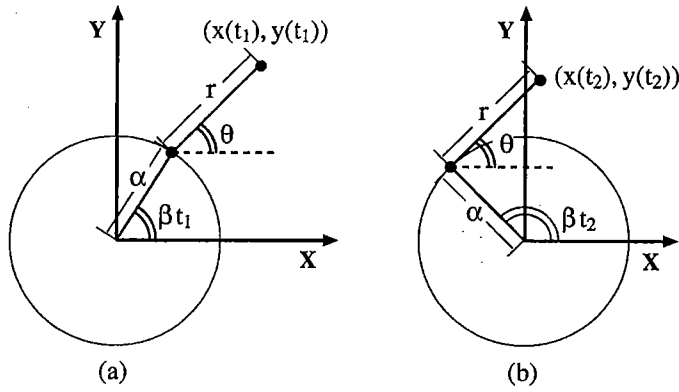


Figure 3. Cartesian coordinates of the point that has polar coordinates (r, θ) relative to the observation point $(\alpha \cos(\beta t), \alpha \sin(\beta t))$ (a) at $t = t_1$ (b) at $t = t_2 > t_1$.

It follows immediately that

$$x(t) = \alpha \cos(\beta t) + r \cos \theta, \quad (8)$$

$$y(t) = \alpha \sin(\beta t) + r \sin \theta, \quad (9)$$

which lead to

$$\frac{x(t)^2 + y(t)^2}{\delta^2} = \frac{r^2}{\delta^2} + 2 \frac{\alpha r}{\delta} \cos(\theta - \beta t) + \frac{\alpha^2}{\delta^2}. \quad (10)$$

Hence

$$\begin{aligned} e^{-(x^2+y^2)/\delta^2} &= e^{-\frac{r^2}{\delta^2}} e^{-2\frac{\alpha r}{\delta} \cos(\theta - \beta t) - \frac{\alpha^2}{\delta^2}} \\ &= e^{-\frac{r^2}{\delta^2}} \left[1 - 2\frac{\alpha r}{\delta} \cos(\theta - \beta t) + O(\delta^2) \right]. \end{aligned} \quad (11)$$

The vorticity at (r, θ) relative to the observation point $(\alpha \cos(\beta t), \alpha \sin(\beta t))$ is

$$\tilde{\omega}\left(\frac{r}{\delta}, \theta, s, t\right) = \frac{1}{\delta^2} e^{-(x^2+y^2)/\delta^2} = \frac{1}{\delta^2} e^{-r^2/\delta^2} - \frac{1}{\delta} \left[\frac{2\alpha r}{\delta^2} \cos(\theta - \beta t) \right] + O(1). \quad (12)$$

Therefore the vorticity distribution observed relative to $(\alpha \cos(\beta t), \alpha \sin(\beta t), 0)$ is

$$\tilde{\eta}^{(0)}\left(\frac{r}{\delta}, s, t\right) = e^{-r^2/\delta^2}, \quad (13)$$

$$\tilde{\eta}^{(1)}\left(\frac{r}{\delta}, \theta, s, t\right) = -\frac{2\alpha r}{\delta^2} \cos(\theta - \beta t). \quad (14)$$

Obviously, $\tilde{\eta}^{(1)}$ given by (14) is not quasi-steady since $\frac{\partial \tilde{\eta}^{(1)}}{\partial t} \sim \beta \sim \frac{1}{\delta^2}$.

From the definition of the line of stagnation points, it is clear that the velocity of a thin filament is the velocity of the line of stagnation points, which is also the fluid velocity at the line of stagnation points.

To simulate the motion of a vortex filament, we need to know the velocity of the filament which is the fluid velocity at the line of the stagnation points induced by the vortex filament plus the external velocity field if any. We first try to evaluate the induced velocity given by the three dimensional Biot-Savart integral

$$\begin{aligned} \mathbf{v}(\mathbf{x}) &= \frac{1}{4\pi} \int \frac{\mathbf{x}' - \mathbf{x}}{|\mathbf{x}' - \mathbf{x}|^3} \times \mathbf{P}(\mathbf{x}') d\mathbf{x}' \\ &= \frac{1}{4\pi} \left[\int_{R^3 \setminus B_1} \frac{\mathbf{x}' - \mathbf{x}}{|\mathbf{x}' - \mathbf{x}|^3} \times \mathbf{P}(\mathbf{x}') d\mathbf{x}' + \int_{B_1} \frac{\mathbf{x}' - \mathbf{x}}{|\mathbf{x}' - \mathbf{x}|^3} \times \mathbf{P}(\mathbf{x}') d\mathbf{x}' \right] \\ &\stackrel{\text{def}}{=} \mathbf{v}_{\text{nonlocal}} + \mathbf{v}_{\text{local}}, \end{aligned} \quad (15)$$

where B_1 is a ball of radius δ_B centered at \mathbf{x} (Fig. 4) with radius $\delta_B \sim \sqrt{R\delta}$, R is a typical radius of curvature of the filament curve and δ is the core size, and $\mathbf{P}(\mathbf{x})$ is the vorticity distribution.

Assume $\mathbf{P}(\mathbf{x})$ satisfies assumptions (a) and (b) :

$$\begin{aligned} \mathbf{P}(\mathbf{x}) &= \frac{1}{\delta^2} \left[\eta^{(0)}\left(\frac{r}{\delta}, s, t\right) \mathbf{e}_\theta + \zeta^{(0)}\left(\frac{r}{\delta}, s, t\right) \mathbf{e}_t \right] \\ &+ \frac{1}{\delta} \left[\xi^{(1)}\left(\frac{r}{\delta}, \theta, s, t\right) \mathbf{e}_r + \eta^{(1)}\left(\frac{r}{\delta}, \theta, s, t\right) \mathbf{e}_\theta + \zeta^{(1)}\left(\frac{r}{\delta}, \theta, s, t\right) \mathbf{e}_t \right] \\ &+ O(1). \end{aligned} \quad (16)$$

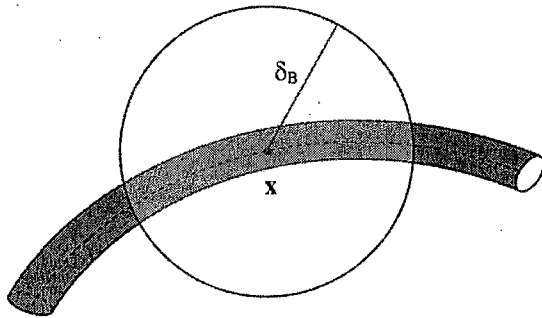


Figure 4. Contribution to the velocity at \mathbf{x} by the vortex filament is divided into two parts: $\mathbf{v}_{\text{local}}$ is the contribution from the part of vortex filament inside a ball of radius δ_B centered at \mathbf{x} whereas $\mathbf{v}_{\text{nonlocal}}$ is the contribution from the rest of the vortex filament.

Here we should point out that $\mathbf{P}(\mathbf{x})$ in the above is not necessarily the physical vorticity distribution. Later, we need to take $\mathbf{P}(\mathbf{x})$ as a numerical vorticity distribution which is not divergence free but has the same expansion form as the physical vorticity distribution ω in equation (2). That is why we use the notation $\mathbf{P}(\mathbf{x})$ instead of $\omega(\mathbf{x})$. Numerical vorticity distribution will be defined when we discuss the thin tube method in next section.

Ignoring the velocity component in the tangential direction which is irrelevant for the filament geometric evolution, we have

$$\mathbf{v}_{nonlocal} = \frac{\Gamma}{4\pi} \left(\int_{-\infty}^{-\delta_B} + \int_{\delta_B}^{\infty} \right) \frac{\mathbf{x}(\tilde{s} + \tilde{s}') - \mathbf{x}(\tilde{s})}{|\mathbf{x}(\tilde{s} + \tilde{s}') - \mathbf{x}(\tilde{s})|^3} \times \frac{\partial}{\partial \tilde{s}} \mathbf{x}(\tilde{s} + \tilde{s}') d\tilde{s}' + O(\delta_B + \delta/\delta_B), \quad (17)$$

$$\mathbf{v}_{local} = \frac{\Gamma}{4\pi} \left[\log\left(\frac{2\delta_B}{\delta}\right) + C \right] (\kappa \mathbf{b}) + O(\delta_B + \delta/\delta_B), \quad (18)$$

$$C = - \left(\frac{1}{2} + \frac{2\pi}{\Gamma} \int_0^{\infty} \left[\frac{1}{\kappa} \zeta_{11}^{(1)} + \bar{r} \ln \bar{r} \zeta^{(0)} \right] d\bar{r} \right), \quad (19)$$

where \bar{r} is the stretched radial coordinate $\bar{r} = r/\delta$, $\zeta_{11}^{(1)}$ is the first cosine Fourier component with respect to θ of the first-order axial vorticity, i.e. ,

$$\zeta_{11}^{(1)} = \frac{1}{\pi} \int_0^{2\pi} \zeta^{(1)} \cos \theta d\theta. \quad (20)$$

In equation (17) \tilde{s} is the current arclength. In equation (18) κ is the curvature, \mathbf{b} is the binormal vector, and $\kappa \mathbf{b}$ can be written as

$$\kappa \mathbf{b} = \mathbf{t} \times \mathbf{n} = \frac{\partial}{\partial \tilde{s}} \mathbf{x}(\tilde{s}) \times \frac{\partial^2}{\partial \tilde{s}^2} \mathbf{x}(\tilde{s}). \quad (21)$$

Here we have reparametrized $\mathbf{x}(s, t)$ using the current arclength \tilde{s} . Combining (15), (17) and (18), one has

$$\mathbf{v}(\tilde{s}) = \frac{\Gamma}{4\pi} \left[\log\left(\frac{2\delta_B}{\delta}\right) + C \right] (\kappa \mathbf{b}) + \frac{\Gamma}{4\pi} \left(\int_{-\infty}^{-\delta_B} + \int_{\delta_B}^{\infty} \right) \frac{\mathbf{x}(\tilde{s} + \tilde{s}') - \mathbf{x}(\tilde{s})}{|\mathbf{x}(\tilde{s} + \tilde{s}') - \mathbf{x}(\tilde{s})|^3} \times \frac{\partial}{\partial \tilde{s}} \mathbf{x}(\tilde{s} + \tilde{s}') d\tilde{s}' + o(1). \quad (22)$$

Now the constant C given by equation (19) remains to be calculated. If $\mathbf{P}(\mathbf{x})$ represents a numerical vorticity distribution, from the discussion of the numerical vorticity distribution in next section, we see that $\zeta_{11}^{(1)}$ and $\zeta^{(0)}$ can be explicitly expressed in terms

of the cut-off function and the curvature of the filament. The constant C can be calculated in a straightforward way.

For physical vorticity distribution, we now examine Euler's equation in vorticity form

$$\omega_t + (\mathbf{v} \cdot \nabla)\omega = (\omega \cdot \nabla)\mathbf{v}. \quad (23)$$

Insertion of equation (2) into equation (23) first shows that the leading two terms in δ express a balance of vorticity advection and vortex stretching.

$$(\tilde{\mathbf{v}} \cdot \nabla)\omega = (\omega \cdot \nabla)\tilde{\mathbf{v}}(1 + O(\delta^2)), \quad (24)$$

where $\tilde{\mathbf{v}}$ is the relative velocity in the curve attached reference system. Note that the time derivative has been dropped out since we have assumed the core structure is quasi-steady. It turns out that the leading order equations of (24) are satisfied by any arbitrary axisymmetric leading order core structure. This implies that the leading order core structure can not be determined from equation (24). So $\eta^{(0)}$ and $\zeta^{(0)}$ have to be supplied. The first order equations of (24) allows us to write the constant C in terms of the leading order core structure $\eta^{(0)}$ and $\zeta^{(0)}$:

$$C = \lim_{\bar{r} \rightarrow \infty} \left(\frac{4\pi^2}{\Gamma^2} \int_0^{\bar{r}} r' (v^{(0)}(r'))^2 dr' - \ln \bar{r} \right) - \frac{1}{2} - \frac{8\pi^2}{\Gamma^2} \int_0^{\infty} r' [\omega^{(0)}(r')]^2 dr', \quad (25)$$

where

$$v^{(0)}(\bar{r}) = \frac{1}{\bar{r}} \int_0^{\bar{r}} r' \zeta^{(0)}(r') dr', \quad (26)$$

$$\omega^{(0)}(\bar{r}) = \int_{\bar{r}}^{\infty} \eta^{(0)}(r') dr'. \quad (27)$$

For a Gaussian axial vorticity distribution, one has

$$\eta^{(0)}(\bar{r}) = 0, \quad (28)$$

$$\zeta^{(0)}(\bar{r}) = \frac{e^{-\bar{r}^2}}{\pi}, \quad (29)$$

$$\text{and } C = -0.558. \quad (30)$$

Finally, to conclude the thin tube model, we want to emphasize that the quasi-steady core structure assumption (b) is very important. It allows us to define the line of

stagnation points, and to calculate the constant C in terms of the leading order core distribution.

3. Review of Klein and Knio's method

In the previous section we introduced the thin tube model (22). Before presenting our method to solve equation (22), we quickly review the numerical method by Klein and Knio [10] and point out the numerical difficulties in their scheme.

Klein and Knio's method is based on the vortex method with only one filament, which is called the thin tube method [9]. The basic idea in the thin tube method is to use a single chain of overlapping vortex elements to represent the slender physical vortex. Each element is a circular cylinder characterized by a circulation Γ and by two sets of Lagrangian coordinates which represent the endpoints of the associated line segment. The Lagrangian points move with the fluid and can be denoted by \mathbf{x}_i , $i = 1, 2, \dots, N$. The vortex elements are ordered so that the indices increase in the direction of the vorticity. Therefore, the discretized vorticity can be written as

$$\omega(\mathbf{x}, t) = \sum_{i=1}^N \Gamma \delta \mathbf{x}_i(t) K_\delta(\mathbf{x} - \mathbf{x}_{i+\frac{1}{2}}(t)). \quad (31)$$

Here K_δ is a smooth approximation to the Dirac delta function with a cutoff radius δ and formed by

$$K_\delta(\mathbf{x}) = \frac{1}{\delta^3} K\left(\frac{|\mathbf{x}|}{\delta}\right), \quad (32)$$

and

$$\mathbf{x}_{j+\frac{1}{2}} = \frac{1}{2} (\mathbf{x}(\tilde{s}_j) + \mathbf{x}(\tilde{s}_{j+1})), \quad (33)$$

$$\delta \mathbf{x}_{j+\frac{1}{2}} = \mathbf{x}(\tilde{s}_{j+1}) - \mathbf{x}(\tilde{s}_j), \quad (34)$$

denote respectively the length and center of the i -th vortex element. The smoothing function $K(\mathbf{x})$ is chosen so as to enhance accuracy [13].

The velocity at a point \mathbf{x} can be obtained by inserting (31) into (1) and performing the integration. The result is the following desingularized version of the Biot-Savart law:

$$\mathbf{v}^{ttm}(\tilde{s}) = \frac{\Gamma}{4\pi} \sum_{j=-\infty}^{+\infty} \frac{\mathbf{x}_{j+\frac{1}{2}} - \mathbf{x}(\tilde{s})}{|\mathbf{x}_{j+\frac{1}{2}} - \mathbf{x}(\tilde{s})|^3} \times \delta \mathbf{x}_{j+\frac{1}{2}} f(|\mathbf{x}_{j+\frac{1}{2}} - \mathbf{x}(\tilde{s})|/\delta^{ttm}), \quad (35)$$

where ttm stands for "thin tube method", and $f(r)$ is the velocity cut-off function corresponding to the vorticity smoothing kernel:

$$f(r) = 4\pi \int_0^r \bar{r}^2 K(\bar{r}) d\bar{r}. \quad (36)$$

To satisfy the overlapping condition, we require that

$$|\delta \mathbf{x}_{j+\frac{1}{2}}| \ll \delta^{ttm}. \quad (37)$$

Conversely, given a spatial discretization and a velocity cut-off function f , the corresponding discrete vorticity distribution is

$$\mathbf{P}(\mathbf{x}) = \frac{\Gamma}{(\delta^{ttm})^3} \sum_{j=-\infty}^{+\infty} g\left(\frac{|\mathbf{x} - \mathbf{x}_{j+\frac{1}{2}}|}{\delta^{ttm}}\right) \delta \mathbf{x}_{j+\frac{1}{2}}, \quad (38)$$

where $g(r) = \frac{f'(r)}{4\pi r^2}$. As $|\delta \mathbf{x}_{j+\frac{1}{2}}|/\delta^{ttm}$ goes to zero, one has

$$\mathbf{P}(\mathbf{x}) = \frac{\Gamma}{\delta^3} \int_{-\infty}^{+\infty} g\left(\frac{|\mathbf{x} - \mathbf{x}(\bar{s})|}{\delta}\right) \frac{d\mathbf{x}(\bar{s})}{d\bar{s}} d\bar{s}. \quad (39)$$

Here for simplicity we have dropped the superscript "tm". $\mathbf{P}(\mathbf{x})$ is called the numerical vorticity distribution. It can be shown that $\mathbf{P}(\mathbf{x})$ has the asymptotic expansion form

$$\mathbf{P}(\mathbf{x}) = \frac{1}{\delta^2} \zeta^{(0),ttm}\left(\frac{r}{\delta}\right) \mathbf{e}_t + \frac{1}{\delta} \cos \theta \zeta_{11}^{(1),ttm}\left(\frac{r}{\delta}\right) \mathbf{e}_t + O(1) \quad (40)$$

with

$$\zeta^{(0),ttm}(r) = \Gamma \int_{-\infty}^{+\infty} g(\sqrt{r^2 + z^2}) dz, \quad (41)$$

$$\zeta^{(1),ttm}(r) = -\frac{\Gamma \kappa}{2} \int_{-\infty}^{+\infty} \frac{rz^2}{\sqrt{r^2 + z^2}} g'(\sqrt{r^2 + z^2}) dz. \quad (42)$$

Recall that the derivation of equation (22) in the previous section requires only that $\mathbf{P}(\mathbf{x})$ satisfies assumption (a) and (b). It does not require $\mathbf{P}(\mathbf{x})$ to be a physical vorticity distribution. Applying equation (22) to the numerical vorticity distribution $\mathbf{P}(\mathbf{x})$ in equation (40), we obtain

$$\begin{aligned} \mathbf{v}^{ttm}(\bar{s}) &= \frac{\Gamma}{4\pi} \left[\log\left(\frac{2\delta_B}{\delta^{ttm}}\right) + C^{ttm} \right] (\kappa \mathbf{b}) \\ &+ \frac{\Gamma}{4\pi} \left(\int_{-\infty}^{-\delta_B} + \int_{\delta_B}^{+\infty} \right) \frac{\mathbf{x}(\bar{s} + \bar{s}') - \mathbf{x}(\bar{s})}{|\mathbf{x}(\bar{s} + \bar{s}') - \mathbf{x}(\bar{s})|^3} \times \frac{\partial}{\partial \bar{s}} \mathbf{x}(\bar{s} + \bar{s}') d\bar{s}' + o(1), \end{aligned} \quad (43)$$

where the constant C^{tm} is determined by functions $\zeta^{(0),tm}$ and $\zeta_{11}^{(1),tm}$ which are given in equations (41) and (42).

Applying equation (22) to the physical vorticity distribution $\omega(\mathbf{x})$ in equation (2) yields

$$\begin{aligned} \mathbf{v}^{real}(\bar{s}) &= \frac{\Gamma}{4\pi} \left[\log\left(\frac{2\delta_B}{\delta_{real}}\right) + C^{real} \right] (\kappa \mathbf{b}) \\ &+ \frac{\Gamma}{4\pi} \left(\int_{-\delta_B}^{-\infty} + \int_{\delta_B}^{+\infty} \right) \frac{\mathbf{x}(\bar{s} + \bar{s}') - \mathbf{x}(\bar{s})}{|\mathbf{x}(\bar{s} + \bar{s}') - \mathbf{x}(\bar{s})|^3} \times \frac{\partial}{\partial \bar{s}'} \mathbf{x}(\bar{s} + \bar{s}') d\bar{s}' + o(1). \end{aligned} \quad (44)$$

Comparing equation (43) with equation (44), one immediately obtains

$$\mathbf{v}^{real}(\bar{s}) = \mathbf{v}^{tm}(\bar{s}) + \frac{\Gamma}{4\pi} \left[\log\left(\frac{\delta^{tm}}{\delta_{real}}\right) + C^{real} - C^{tm} \right] (\kappa \mathbf{b}) + o(1) \quad (45)$$

$$\stackrel{\text{def}}{=} \mathbf{v}^{tm}(\bar{s}) + \text{correction term}. \quad (46)$$

In Klein and Knio's numerical method, $\mathbf{v}^{real}(\bar{s})$ is obtained by first calculating $\mathbf{v}^{tm}(\bar{s})$ using equation (35) and then adding a correction term to it as in equation (46). In this method, the space step $\delta \mathbf{x}_{j+\frac{1}{2}} = \mathbf{x}_{j+1} - \mathbf{x}_j$ is strictly restricted by the overlapping requirement

$$|\delta \mathbf{x}_{j+\frac{1}{2}}| \ll \delta^{tm}. \quad (47)$$

If the physical core radius δ^{real} is small compared to R , a typical radius of curvature of the filament curve, the error associated with the asymptotic expansion for the physical vorticity distribution is small. In this case, we are faced with some numerical difficulties:

1. If we choose δ^{tm} comparable to the physical core size δ^{real} , then to satisfy the overlapping requirement (47), we have to use a space step much smaller than the core radius δ^{real} . It results in a lot more numerical nodes than it is necessary to represent the filament curve geometrically. In this way the computation could be awfully expensive for very slender vortex filament (e.g., superfluid vortex filaments where the physical core radius δ^{real} is of the order of $\sim 1 \text{ \AA}$).
2. If we instead choose a space step $|\delta \mathbf{x}_{j+\frac{1}{2}}|$ according to the filament geometry, then to satisfy the overlapping condition, we have to use a numerical core size much larger than the space step: $\delta^{tm} \gg |\delta \mathbf{x}_{j+\frac{1}{2}}|$. This choice could lead to a large error in the asymptotic expansion for the numerical vorticity distribution because the validity of the asymptotic expansion depends on the assumption that $\delta^{tm} \ll R$. This large error in equation (43) in turn could cause a large error in the calculated filament velocity given by equation (44).

To overcome these numerical difficulties, we propose an efficient numerical method for solving the thin tube model (22).

4. A fast method for thin vortex filament

In this section we present a fast method for thin vortex filament. In our method, we evaluate the velocity in equation (22) directly instead of using the thin tube method. The advantage of this method is that there is no need to satisfy the overlapping condition. Thus, the space step is no longer restricted by the physical core size δ . Rather it is determined by the smoothness of the filament curve.

We start by rewriting equation (22) in a slightly different form. Splitting the integral $\int_{-\infty}^{-\delta_B}$ into two parts and then doing the same for the integrals $\int_{\delta_B}^{\infty}$, one obtains

$$\begin{aligned}
\mathbf{v}(\bar{s}) &= \frac{\Gamma}{4\pi} \left[\log\left(\frac{2\delta_B}{\delta}\right) + C \right] (\kappa \mathbf{b}) \\
&+ \frac{\Gamma}{4\pi} \left(\int_{-\infty}^{-\delta_B} + \int_{\delta_B}^{+\infty} \right) \frac{\mathbf{x}(\bar{s} + \bar{s}') - \mathbf{x}(\bar{s})}{|\mathbf{x}(\bar{s} + \bar{s}') - \mathbf{x}(\bar{s})|^3} \times \frac{\partial}{\partial \bar{s}} \mathbf{x}(\bar{s} + \bar{s}') d\bar{s}' + o(1) \\
&= \frac{\Gamma}{4\pi} \left[\log\left(\frac{2\delta_B}{\delta}\right) + C \right] (\kappa \mathbf{b}) \\
&+ \frac{\Gamma}{4\pi} \left(\int_{-\rho_1}^{-\delta_B} + \int_{\delta_B}^{\rho_2} \right) \left[\frac{\mathbf{x}(\bar{s} + \bar{s}') - \mathbf{x}(\bar{s})}{|\mathbf{x}(\bar{s} + \bar{s}') - \mathbf{x}(\bar{s})|^3} \times \frac{\partial}{\partial \bar{s}} \mathbf{x}(\bar{s} + \bar{s}') \right] d\bar{s}' \\
&+ \frac{\Gamma}{4\pi} \left(\int_{-\infty}^{-\rho_1} + \int_{\rho_2}^{\infty} \right) \left[\frac{\mathbf{x}(\bar{s} + \bar{s}') - \mathbf{x}(\bar{s})}{|\mathbf{x}(\bar{s} + \bar{s}') - \mathbf{x}(\bar{s})|^3} \times \frac{\partial}{\partial \bar{s}} \mathbf{x}(\bar{s} + \bar{s}') \right] d\bar{s}' + o(1),
\end{aligned} \tag{48}$$

where ρ_1 and ρ_2 are of the order of $O(R)$. The power series expansion yields

$$|\mathbf{x}(\bar{s} + \bar{s}') - \mathbf{x}(\bar{s})|^3 = |\bar{s}'|^3 \left[1 + O(|\bar{s}'|) \right], \tag{49}$$

$$\mathbf{x}(\bar{s} + \bar{s}') - \mathbf{x}(\bar{s}) = \frac{\partial}{\partial \bar{s}} \mathbf{x}(\bar{s}) \bar{s}' + \frac{1}{2} \frac{\partial^2}{\partial \bar{s}^2} \mathbf{x}(\bar{s}) (\bar{s}')^2 + \frac{1}{6} \frac{\partial^3}{\partial \bar{s}^3} \mathbf{x}(\bar{s}) (\bar{s}')^3 + O(|\bar{s}'|^4), \tag{50}$$

$$\text{and } \frac{\partial}{\partial \bar{s}} \mathbf{x}(\bar{s} + \bar{s}') = \frac{\partial}{\partial \bar{s}} \mathbf{x}(\bar{s}) + \frac{\partial^2}{\partial \bar{s}^2} \mathbf{x}(\bar{s}) \bar{s}' + \frac{1}{2} \frac{\partial^3}{\partial \bar{s}^3} \mathbf{x}(\bar{s}) (\bar{s}')^2 + O(|\bar{s}'|^3), \tag{51}$$

which lead to

$$\begin{aligned}
(\mathbf{x}(\bar{s} + \bar{s}') - \mathbf{x}(\bar{s})) \times \frac{\partial}{\partial \bar{s}} \mathbf{x}(\bar{s} + \bar{s}') &= \frac{1}{2} \frac{\partial}{\partial \bar{s}} \mathbf{x}(\bar{s}) \times \frac{\partial^2}{\partial \bar{s}^2} \mathbf{x}(\bar{s}) (\bar{s}')^2 \\
&+ \frac{1}{3} \frac{\partial}{\partial \bar{s}} \mathbf{x}(\bar{s}) \times \frac{\partial^3}{\partial \bar{s}^3} \mathbf{x}(\bar{s}) (\bar{s}')^3 + O(|\bar{s}'|^4).
\end{aligned} \tag{52}$$

Combining (49) and (52), one finally obtains

$$\frac{\mathbf{x}(\bar{s} + \bar{s}') - \mathbf{x}(\bar{s})}{|\mathbf{x}(\bar{s} + \bar{s}') - \mathbf{x}(\bar{s})|^3} \times \frac{\partial}{\partial \bar{s}} \mathbf{x}(\bar{s} + \bar{s}') = \frac{1}{2} \frac{1}{|\bar{s}'|} (\kappa \mathbf{b}) + \frac{1}{3} \frac{\partial}{\partial \bar{s}} \mathbf{x}(\bar{s}) \times \frac{\partial^3}{\partial \bar{s}^3} \mathbf{x}(\bar{s}) \text{sign}(\bar{s}') + O(|\bar{s}'|). \tag{53}$$

Hence the integrand (53) in equation (48) is dominated by $\frac{1}{2} \frac{1}{|\bar{s}'|} \kappa \mathbf{b}$ as \bar{s}' goes to zero. Applying a numerical integration method directly to this singular integrand will result in

very low order of accuracy. Consequently very small space step is required to achieve a reasonable accuracy. To eliminate this singularity, we extract out the singular part $\frac{1}{2} \frac{1}{|\tilde{s}'|} \kappa \mathbf{b}$ and integrate it exactly.

To make the expression of $\mathbf{v}(\tilde{s})$ easy to read, we introduce two functions $B_1(\tilde{s}, \tilde{s}')$ and $B_2(\tilde{s}, \tilde{s}')$ as follows:

$$B_1(\tilde{s}, \tilde{s}') \stackrel{\text{def}}{=} \frac{\mathbf{x}(\tilde{s} + \tilde{s}') - \mathbf{x}(\tilde{s})}{|\mathbf{x}(\tilde{s} + \tilde{s}') - \mathbf{x}(\tilde{s})|^3} \times \frac{\partial}{\partial \tilde{s}} \mathbf{x}(\tilde{s} + \tilde{s}'), \quad (54)$$

$$B_2(\tilde{s}, \tilde{s}') \stackrel{\text{def}}{=} \frac{\mathbf{x}(\tilde{s} + \tilde{s}') - \mathbf{x}(\tilde{s})}{|\mathbf{x}(\tilde{s} + \tilde{s}') - \mathbf{x}(\tilde{s})|^3} \times \frac{\partial}{\partial \tilde{s}} \mathbf{x}(\tilde{s} + \tilde{s}') - \frac{1}{2} \frac{1}{|\tilde{s}'|} (\kappa \mathbf{b}). \quad (55)$$

With $B_1(\tilde{s}, \tilde{s}')$ and $B_2(\tilde{s}, \tilde{s}')$ defined as above, we can write $\mathbf{v}(\tilde{s})$ as

$$\begin{aligned} \mathbf{v}(\tilde{s}) = & \frac{\Gamma}{4\pi} \left[\log(2) \frac{\sqrt{\rho_1 \rho_2}}{\delta} + C \right] (\kappa \mathbf{b}) + \frac{\Gamma}{4\pi} \left(\int_{-\rho_1}^0 + \int_0^{\rho_2} \right) B_2(\tilde{s}, \tilde{s}') d\tilde{s}' \\ & + \frac{\Gamma}{4\pi} \left(\int_{-\infty}^{-\rho_1} + \int_{\rho_2}^{+\infty} \right) B_1(\tilde{s}, \tilde{s}') d\tilde{s}' + o(1). \end{aligned} \quad (56)$$

It is easy to see that

- $B_2(\tilde{s}, \tilde{s}')$ has no numerical singularity in $(-\rho_1, 0)$ or $(0, \rho_2)$;
- $B_1(\tilde{s}, \tilde{s}')$ has no numerical singularity in $(-\infty, -\rho_1)$ or (ρ_2, ∞) .

Later we will show that with the help of the periodic boundary conditions, the integral on the infinite interval (ρ_2, ∞) can be converted to an integral on a finite interval. With the singularity removed, the accuracy of the numerical integration is determined by the quadrature and the smoothness of the filament curve. It is not in any way affected by the physical core size. Therefore, the space step size in numerical integration is not restricted by the physical core size. It is only restricted by the smoothness of the filament curve. For the same filament geometry, no matter how small the physical core size is, we can always use the same space discretization without suffering a loss of accuracy when the core size goes to zero.

Now we describe our method in more details.

Let $\mathbf{x}_1, \mathbf{x}_2, \dots, \mathbf{x}_N$ be N numerical nodes representing one period of a periodic filament curve at time $t = t^n$. We want to calculate the induced velocity at $\mathbf{x}_1, \mathbf{x}_2, \dots, \mathbf{x}_N$ by this periodic vortex filament (here periodicity means $\mathbf{x}_{i+N} = \mathbf{x}_i + (L, 0, 0)$ and L is the period). Once we know how to calculate the induced velocity, we can use an ODE solver to advance the filament curve from $t = t^n$ to $t = t^n + \Delta t$. The procedure of evaluating the induced velocity consists of three steps:

Step 1. Calculating the current arclength from \mathbf{x}_i to \mathbf{x}_{i+1} . Let

$$l_{i+\frac{1}{2}} = |\mathbf{x}_{i+1} - \mathbf{x}_i|, \quad (57)$$

$$l_i = |\mathbf{x}_{i+1} - \mathbf{x}_{i-1}|/2, \quad (58)$$

$$C_i = \frac{l_{i+\frac{1}{2}} + l_{i-\frac{1}{2}} - 2l_i}{8l_i^3 - l_{i+\frac{1}{2}}^3 - l_{i-\frac{1}{2}}^3}, \quad (59)$$

$$\text{and } C_{i+\frac{1}{2}} = \frac{1}{2}(C_i + C_{i+1}). \quad (60)$$

The current arclength from \mathbf{x}_i to \mathbf{x}_{i+1} is

$$\Delta \tilde{s}_{i+\frac{1}{2}} = l_{i+\frac{1}{2}} + C_{i+\frac{1}{2}} l_{i+\frac{1}{2}}^3 + O(l_{i+\frac{1}{2}}^4). \quad (61)$$

Step 2. With the current arclength as the parameter, we recover the filament curve by a periodic cubic spline interpolation. We can calculate $\mathbf{x}(\tilde{s})$, $\frac{\partial}{\partial \tilde{s}} \mathbf{x}(\tilde{s})$, $\frac{\partial^2}{\partial \tilde{s}^2} \mathbf{x}(\tilde{s})$, $\frac{\partial^3}{\partial \tilde{s}^3} \mathbf{x}(\tilde{s})$ for any \tilde{s} from the piecewise cubic polynomials obtained by the periodic spline.

Step 3. Using equation (56), we get the formula for the induced velocity at \mathbf{x}_i :

$$\begin{aligned} \mathbf{v}_i \equiv \mathbf{v}(\tilde{s}_i) &= \frac{\Gamma}{4\pi} \left[\log(2 \frac{\sqrt{\rho_{1,i} \rho_{2,i}}}{\delta}) + C \right] (\kappa_i \mathbf{b}_i) + \frac{\Gamma}{4\pi} \left(\int_{-\rho_{1,i}}^0 + \int_0^{\rho_{2,i}} \right) B_2(\tilde{s}_i, \tilde{s}') d\tilde{s}' \\ &+ \frac{\Gamma}{4\pi} \left(\int_{-\infty}^{-\rho_{1,i}} + \int_{\rho_{2,i}}^{+\infty} \right) B_1(\tilde{s}_i, \tilde{s}') d\tilde{s}' \end{aligned} \quad (62)$$

where

$$B_1(\tilde{s}_i, \tilde{s}) = \frac{\mathbf{x}(\tilde{s}_i + \tilde{s}') - \mathbf{x}(\tilde{s}_i)}{|\mathbf{x}(\tilde{s}_i + \tilde{s}') - \mathbf{x}(\tilde{s}_i)|^3} \times \frac{\partial}{\partial \tilde{s}} \mathbf{x}(\tilde{s}_i + \tilde{s}'), \quad (63)$$

$$B_2(\tilde{s}_i, \tilde{s}) = B_1(\tilde{s}_i, \tilde{s}) - \frac{1}{2} \frac{1}{|\tilde{s}'|} (\kappa_i \mathbf{b}_i), \quad (64)$$

$$\rho_{1,i} = \tilde{s}_i - \tilde{s}_{i-m_1}, \quad (65)$$

$$\rho_{2,i} = \tilde{s}_{i+m_1} - \tilde{s}_i, \quad (66)$$

and m_1 is an integer satisfying

$$|\tilde{s}_i - \tilde{s}_{i-m_1}| \sim O(R), \quad (67)$$

$$|\tilde{s}_{i+m_1} - \tilde{s}_i| \sim O(R). \quad (68)$$

Writing the integrals as the sum of the integrals on sub-intervals between two adjacent numerical nodes, we obtain

$$\begin{aligned}
\mathbf{v}_i &= \frac{\Gamma}{4\pi} \left[\log(2) \frac{\sqrt{\rho_{1,i} \rho_{2,i}}}{\delta} + C \right] (\kappa_i \mathbf{b}_i) \\
&+ \frac{\Gamma}{4\pi} \left(\sum_{j=-m_1}^{-1} + \sum_{j=0}^{m_1-1} \right) \int_{\tilde{s}_{i+j-\tilde{s}_i}}^{\tilde{s}_{i+j+1}-\tilde{s}_i} B_2(\tilde{s}_i, \tilde{s}') d\tilde{s}' \\
&+ \frac{\Gamma}{4\pi} \left(\sum_{j=-N/2}^{-m_1-1} + \sum_{j=m_1}^{N/2-1} \right) \int_{\tilde{s}_{i+j-\tilde{s}_i}}^{\tilde{s}_{i+j+1}-\tilde{s}_i} B_1(\tilde{s}_i, \tilde{s}') d\tilde{s}' \\
&+ \frac{\Gamma}{4\pi} \sum_{j=-N/2}^{N/2-1} \sum_{k=\pm 1}^{\pm\infty} \int_{\tilde{s}_{i+j+kN-\tilde{s}_i}}^{\tilde{s}_{i+j+kN+1}-\tilde{s}_i} B_1(\tilde{s}_i, \tilde{s}') d\tilde{s}'.
\end{aligned} \tag{69}$$

In expression (69), each integral can be approximated by trapezoidal rule or high order Gaussian quadrature. For example,

$$\int_{\tilde{s}_{i+j-\tilde{s}_i}}^{\tilde{s}_{i+j+1}-\tilde{s}_i} B_1(\tilde{s}_i, \tilde{s}') d\tilde{s}' \approx \frac{1}{2} \Delta \tilde{s}_{i+j+\frac{1}{2}} [B_1(\tilde{s}_i, \tilde{s}_{i+j-\tilde{s}_i}) + B_1(\tilde{s}_i, \tilde{s}_{i+j+1-\tilde{s}_i})]. \tag{70}$$

The last term in equation (69) needs special treatments since it contains an infinite sum of integrals. Applying trapezoidal rule to each integral, one can rewrite the infinite sum as

$$\begin{aligned}
&\sum_{k=\pm 1}^{\pm\infty} \int_{\tilde{s}_{i+j+kN-\tilde{s}_i}}^{\tilde{s}_{i+j+kN+1}-\tilde{s}_i} B_1(\tilde{s}_i, \tilde{s}') d\tilde{s}' \\
&\approx \frac{1}{2} \sum_{k=\pm 1}^{\pm\infty} \Delta \tilde{s}_{i+j+\frac{1}{2}} [B_1(\tilde{s}_i, \tilde{s}_{i+j+kN-\tilde{s}_i}) + B_1(\tilde{s}_i, \tilde{s}_{i+j+kN+1-\tilde{s}_i})] \\
&= \frac{1}{2} \Delta \tilde{s}_{i+j+\frac{1}{2}} \left[\sum_{k=\pm 1}^{\pm\infty} B_1(\tilde{s}_i, \tilde{s}_{i+j+kN-\tilde{s}_i}) + \sum_{k=\pm 1}^{\pm\infty} B_1(\tilde{s}_i, \tilde{s}_{i+j+kN+1-\tilde{s}_i}) \right].
\end{aligned} \tag{71}$$

With the use of periodic boundary conditions, the infinite sum of function B_1 can be reduced to the evaluation of two functions of two variables:

$$\begin{aligned}
&\sum_{k=\pm 1}^{\pm\infty} B_1(\tilde{s}_i, \tilde{s}_{i+j+kN-\tilde{s}_i}) \\
&= \sum_{k=\pm 1}^{\pm\infty} \frac{\mathbf{x}(\tilde{s}_{i+j+kN}) - \mathbf{x}(\tilde{s}_i)}{|\mathbf{x}(\tilde{s}_{i+j+kN}) - \mathbf{x}(\tilde{s}_i)|^3} \times \frac{\partial}{\partial \tilde{s}} \mathbf{x}(\tilde{s}_{i+j+kN}) \\
&= \sum_{k=\pm 1}^{\pm\infty} \frac{k(L, 0, 0) + \mathbf{x}(\tilde{s}_{i+j}) - \mathbf{x}(\tilde{s}_i)}{|k(L, 0, 0) + \mathbf{x}(\tilde{s}_{i+j}) - \mathbf{x}(\tilde{s}_i)|^3} \times \frac{\partial}{\partial \tilde{s}} \mathbf{x}(\tilde{s}_{i+j}) \\
&= \left[\frac{G(d_1, d_2)}{L^2} (1, 0, 0) + \frac{F(d_1, d_2)}{L^3} (\mathbf{x}(\tilde{s}_{i+j}) - \mathbf{x}(\tilde{s}_i)) \right] \times \frac{\partial}{\partial \tilde{s}} \mathbf{x}(\tilde{s}_{i+j})
\end{aligned} \tag{72}$$

where

$$d_1 = x(\tilde{s}_{i+j}) - x(\tilde{s}_i), \quad (73)$$

$$d_2 = [y(\tilde{s}_{i+j}) - y(\tilde{s}_i)]^2 + [z(\tilde{s}_{i+j}) - z(\tilde{s}_i)]^2, \quad (74)$$

$$F(d_1, d_2) = \sum_{k=\pm 1}^{\pm\infty} \frac{1}{[(k+d_1)^2 + d_2]^{3/2}}, \quad (75)$$

$$G(d_1, d_2) = \sum_{k=\pm 1}^{\pm\infty} \frac{k}{[(k+d_1)^2 + d_2]^{3/2}}. \quad (76)$$

Functions F and G are independent of the filament geometry or the physical core size. They can be evaluated up to machine precision and tabulated once and for all. During the simulations, $F(d_1, d_2)$ and $G(d_1, d_2)$ are calculated by a cubic spline interpolation from the tables containing function values. Once we have \mathbf{v}_i , we can use an ODE solver to advance the filament curve from time $t = t^n$ to $t = t^n + \Delta t$.

The cost for calculating $\{\mathbf{v}_i, i = 1, 2, \dots, N\}$ is $O(N^2)$. To make the algorithm even faster, we can either reduce the cost of calculating $\{\mathbf{v}_i\}$ or use a large time step. In equation (69), the formula for $\{\mathbf{v}_i\}$ includes an infinite sum, which is then expressed in equation (72) in terms of functions F and G . Time step is restricted by the stiffness of the system. Even for the implicit method [14] solving the local induction approximation which is a much simpler model than the thin filament model, the time step Δt is still restricted by $\Delta t \leq O((\Delta s)^2)$. Hence we have to seek a new approach to speed up the algorithm. To do so, we use a fractional step method. In particular, we split the induced velocity \mathbf{v}_i into two parts:

$$\mathbf{v}_i = \mathbf{u}_i + \mathbf{w}_i, \quad (77)$$

where

$$\mathbf{u}_i = \frac{\Gamma}{4\pi} \left[\log \left(2 \frac{\sqrt{r_{1,i} r_{2,i}}}{\delta} \right) + C \right] (\kappa_i \mathbf{b}_i) + \frac{\Gamma}{4\pi} \left(\int_{-r_{1,i}}^0 + \int_0^{r_{2,i}} \right) B_2(\tilde{s}_i, \tilde{s}') d\tilde{s}', \quad (78)$$

$$\begin{aligned} \mathbf{w}_i &= \frac{\Gamma}{4\pi} \left[\log \left(\sqrt{\frac{\rho_{1,i} \rho_{2,i}}{r_{1,i} r_{2,i}}} \right) \right] (\kappa_i \mathbf{b}_i) + \frac{\Gamma}{4\pi} \left(\int_{-\rho_{1,i}}^{-r_{1,i}} + \int_{r_{2,i}}^{\rho_{2,i}} \right) B_2(\tilde{s}_i, \tilde{s}') d\tilde{s}' \\ &+ \frac{\Gamma}{4\pi} \left(\int_{-\infty}^{-\rho_{1,i}} + \int_{\rho_{2,i}}^{\infty} \right) B_1(\tilde{s}_i, \tilde{s}') d\tilde{s}', \end{aligned} \quad (79)$$

$$r_{1,i} = \tilde{s}_i - \tilde{s}_{i-m_2}, \quad (80)$$

$$r_{2,i} = \tilde{s}_{i+m_2} - \tilde{s}_i, \quad (81)$$

and m_2 is a small integer. In fact, \mathbf{u}_i is the velocity induced by the part of the vortex filament from \tilde{s}_{i-m_2} to \tilde{s}_{i+m_2} , and \mathbf{w}_i is the velocity induced by the rest of the vortex filament (Fig. 5). The cost for calculating $\{\mathbf{u}_i\}$ is $O(Nm_2)$, and the cost for calculating $\{\mathbf{w}_i\}$ is $O(N^2)$. When we choose m_2 , we want to make both m_2 and $|\mathbf{w}_i|$ as small as possible. The choice of small m_2 makes it less expensive to calculate $\{\mathbf{u}_i\}$; while small $|\mathbf{w}_i|$ makes it possible to use a large time step for solving $\frac{d}{dt}\mathbf{x} = \mathbf{w}_i(\mathbf{x})$. The ODE system for the motion of the vortex filament can be formally written as

$$\frac{d}{dt}\mathbf{x} = \mathbf{u}(\mathbf{x}) + \mathbf{w}(\mathbf{x}). \quad (82)$$

Strang-type splitting can be employed to solve (82). Let $A(dt_1)$ be a second (or higher) order numerical ODE solver for

$$\frac{d}{dt}\mathbf{x} = \mathbf{u}(\mathbf{x}) \quad (83)$$

with time step dt_1 , and $B(dt_2)$ be a second (or higher) order numerical ODE solver for

$$\frac{d}{dt}\mathbf{x} = \mathbf{w}(\mathbf{x}) \quad (84)$$

with time step dt_2 . A second order numerical ODE solver for equation (82) can be formed by applying operators A and B alternately:

$$\underbrace{A(dt) \cdots A(dt)}_{m_3 \text{ times}} B(2m_3 dt) \underbrace{A(dt) \cdots A(dt)}_{m_3 \text{ times}}. \quad (85)$$

The total cost of (85) is $O(N^2 + N m_2 m_3)$. It advances the vortex filament by $2m_3 dt$ in time direction. The cost per time step dt is $O(\frac{N^2}{m_3} + N m_2)$.

It should be pointed out that, for the system $\frac{d}{dt}\mathbf{x} = \mathbf{u}(\mathbf{x})$, the time step dt of the ODE solver is restricted by the stability requirement

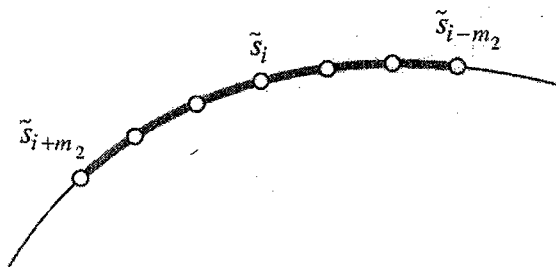


Figure 5. The part of the vortex filament that induces \mathbf{u}_i .

$$dt < O\left((ds)^2 / \log\left[\frac{2ds}{\delta}\right]\right). \quad (86)$$

Since we cannot use large time step, it is important to reduce the cost per time step, which is $O(Nm_2)$. That is why we want to make m_2 as small as possible when we split \mathbf{v} into the sum of \mathbf{u} and \mathbf{w} . For the system $\frac{d}{dt}\mathbf{x} = \mathbf{w}(\mathbf{x})$, the cost per time step is fixed, i.e., $O(N^2)$. The way to speed up is to use large time step. To make this feasible, we want $|\mathbf{w}|$ to be small too. These are the two things we have to take into consideration when choosing m_2 .

As one application, our method can be easily applied to solve the self-induction approximation

$$\frac{\partial \mathbf{x}}{\partial t} = \frac{\partial \mathbf{x}}{\partial s} \times \frac{\partial^2 \mathbf{x}}{\partial s^2}. \quad (87)$$

The cost is $O(N)$ per time step since only the term $\kappa \mathbf{b}$ needs to be evaluated at each node. Compared with Buttke's method [14] for (87), our method has several advantages:

- It is explicit;
- It deals directly with the positions of points on the filament curve instead of the tangent vectors in [14];
- With a cubic spline interpolation, it recovers the filament curve as a piecewise cubic polynomial of the arclength. This allows us to calculate $\frac{\partial \mathbf{x}}{\partial s}$ and $\frac{\partial^2 \mathbf{x}}{\partial s^2}$ with an accuracy of $O((\Delta s)^2)$ even when the numerical points are not smoothly distributed along the curve. By "smoothly distributed", we mean $|\mathbf{x}_{j+1} - \mathbf{x}_j|/|\mathbf{x}_j - \mathbf{x}_{j-1}|$ is a smooth function of j . When we add additional terms (for example Hall Vinen's frictional terms [15]) to the right hand side of the self-induction approximation (87), the new equation might cause a stretching of the vortex filament. To keep the numerical resolution we need to add nodes when the distance between two adjacent nodes is larger than a pre-specified criteria. If this happens, we can expect $|\mathbf{x}_{j+1} - \mathbf{x}_j|/|\mathbf{x}_j - \mathbf{x}_{j-1}|$ to have a jump in the region where we have added new nodes. In that case, the central difference scheme in [14] will lose its second order accuracy. In contrast, in our method $\frac{\partial \mathbf{x}}{\partial s}$ and $\frac{\partial^2 \mathbf{x}}{\partial s^2}$ are always approximated with a true second order accuracy.

In the next section we perform some numerical computations using our fast method just described.

5. Numerical results

In this section we present the numerical results by the thin filament model and compare them with the results by the local induction approximation (LIA). We find several differences between the results by the thin filament model and by LIA. In LIA, the time t has been rescaled by an unknown factor which could be different from one

space point to another. Consequently under LIA, it is impossible to calculate, for example, the velocity of a vortex ring or the frequency of a Kelvin wave. Thus it seems unfair to compare the thin filament model with LIA on any issue which involves a time scale. For this reason, we carried out numerical simulations with both models on the problem of a vortex ring subject to a cosine wave and its sideband perturbations. We plot the amplitudes of the perturbations against the number of rotations the cosine wave has made, instead of against the time t . In this way, the plot is not changed under a rescaling of time t . Comparing the plots for the thin filament model with those for LIA, we find the stability thresholds for the side band perturbation are different for these two models.

Our first numerical example is to simulate the motion of a thin vortex ring. The radius of the ring R is 1, the core size is 10^{-4} , and the circulation Γ is 1. In the simulation, there is no deformation or stretching happened. The vortex ring propagates along its axis at a constant speed 0.85402, which agrees to four digits with the value 0.85400 predicted by the asymptotic formula

$$v_{ring} = \frac{\Gamma}{4R} \left[\log\left(\frac{8R}{\delta}\right) + C \right], \quad (88)$$

where $C = -0.558$ for a second-order Gaussian distribution.

Our second example is a Kelvin wave. Initially the vortex filament is given by

$$\left(x, \alpha \frac{2\pi}{n} \cos(nx), 0\right), \quad (89)$$

where α is a small number. We take $n = 10$, $\alpha = 0.1$, $\delta = 10^{-4}$ and $\Gamma = 1$. The filament rotates around the x -axis with little change in its shape. The rotation frequency given by Lord Kelvin is

$$\omega = \frac{\Gamma}{2\pi\delta^2} \left[1 - \left(1 + n\delta \frac{K_0(n\delta)}{K_1(n\delta)}\right)^{1/2} \right], \quad (90)$$

where K_n is a modified Bessel function of order n . When the core size is much smaller than the wave length, equation (90) can be simplified to

$$\omega = -\frac{\Gamma n^2}{4\pi} \left[\log\left(\frac{2}{n\delta}\right) - \gamma \right], \quad (91)$$

where γ is Euler's constant 0.5772. Substituting the values of n , δ and Γ into (91), we get the theoretical value for the frequency $\omega = 55.893$. The frequency obtained from the numerical simulation is $\omega = 55.87$. They agree with each other very well.

For the third example, we consider the sideband instability on a vortex ring. The sideband instability on a straight line has been studied in [17] and [20]. Even though sideband instability is expected for a vortex ring, numerical simulations have not been done yet. So here we apply our fast method to study the sideband instability on a vortex ring. At time $t = 0$, the unperturbed filament configuration is a cosine wave on a ring $(\cos\theta, \sin\theta, \alpha \frac{2\pi}{n} \cos n\theta)$. The sideband perturbation is a perturbation of the form

$$(0, 0, \varepsilon \alpha \frac{2\pi}{n} [\cos(n+1)\theta + \cos(n-1)\theta]),$$

where ε is a small number. Whether or not the sideband perturbation will grow depends on the initial amplitude of the cosine wave (called carrier) $\alpha \frac{2\pi}{n}$. There is a stability threshold. When α is smaller than the threshold, the side band perturbation does not grow. When α is larger than the threshold, the amplitude of the side band perturbation grows exponentially to a fraction of $\alpha \frac{2\pi}{n}$ and the amplitude of the carrier decreases. After reaching a maximum, the amplitude of the sideband goes back approximately to its initial value and starts over once again. In the simulation, we take $n = 11$, $\varepsilon = 10^{-4}$, and $\Gamma = 1$.

We plot the amplitudes of the carrier and the side band perturbation vs the number of rotations that the carrier has made around the ring. Here all of the amplitudes have been normalized by the wave length of the carrier $\frac{2\pi}{n}$. Fig. 6 show the plots for

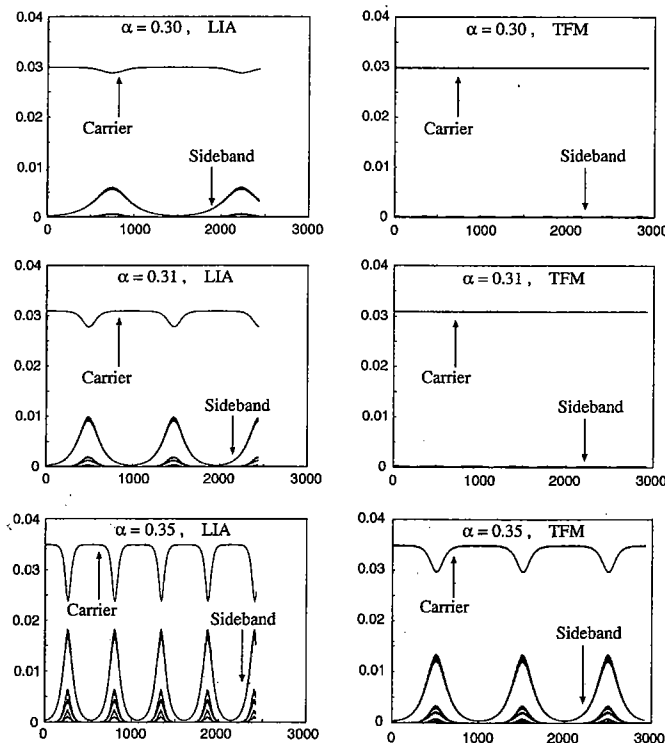


Figure 6. Evolution of sideband perturbation on a vortex ring. Left column: results predicted by the local induction approximation (LIA); right column: results predicted by the thin filament model (TFM). In each panel, the vertical axis shows the normalized amplitudes of the carrier and the side band perturbation; the horizontal axis shows the number of rotations that the carrier has made around the ring.

$\alpha = 0.30, 0.31,$ and 0.35 . Under the LIA, the sideband perturbation is already unstable for $\alpha=0.30$, while, under the thin filament model, it is still stable for $\alpha = 0.31$. For $\alpha = 0.35$, it is unstable for both models. However, for $\alpha = 0.35$, the peak amplitudes that the sideband perturbations can reach and the intervals between two peaks are different. These differences can not be reconciled by a rescaling of time t , since the plots are invariant under such a rescaling.

6. Conclusions

In this paper, a fast method is proposed for simulating the motion of thin vortex filament. The accuracy of the method does not depend on the size of the core radius. Rather it is determined by the smoothness of the filament curve. This property makes our method especially attractive for numerical simulations of very thin filament. To speed up the method even further, we split the velocity field into two parts and use a Strang-type ODE solver to advance the filament. In this way, effective large time step can be used.

7. Acknowledgements

The authors would like to thank Alexandre Chorin for introducing them to vortex dynamics and vortex methods, and for many helpful discussions during this study.

References

1. Crow, S. C., 1970, *AIAA*, 8, 2172.
2. Ting, L., 1971, *Aircraft Wake Turbulence and its detection*, J.H.Olsen, A. Goldburg and M. Rogers (Ed.), Plenum, 11.
3. Widnall, S. E., 1976, *Annu. Fluid Mech.*, 8, 141.
4. Chorin, A. J., 1982, *Comm. Math. Phys.*, 83, 517.
5. Chorin, A. J., and Akao, J., 1991, *Physica D*, 51, 403.
6. Rayfield, G. W., and Reif, F., 1964, *Physical Review*, 136, 1194.
7. Armes, R., and Hama, F., 1965, *Phys. Fluids*, 8, 553.
8. Klein, R., and Majda, A., 1991, *Physica D* 49, 323 .
9. Knio, O. M., and Ghoniem, A. F., 1990, *J. Comput. Phys.*, 86, 75.
10. Klein, R., and Knio, O. M., 1995, *J. Fluid Mech.*, 284, 275.
11. Callegari, A., and Ting, L., 1978, *SIAM J. Appl. Math.*, 15, 148.
12. Klein, R., Knio, O. M., and Ting, L., 1996, *Phys. Fluids*, 8, 2415.
13. Beale, J. T., and Majda, A., 1985, *J. Comput. Phys.*, 58, 188.
14. Buttkke, T. F., 1988, *J. Comput. Phys.*, 76, 301.
15. Hall, H. E., and Vinen, W. F., 1956, *Proc. Roy. Soc. London*, 238, 204.
16. Chorin, A. J., 1993, *Vorticity and Turbulence*, Springer, New York.
17. Samuels, D. C., and Donnelly, R. J., 1990, *Phys. Rev. Lett.*, 64, 1385.
18. Chorin, A. J., 1996, *Computational Fluid Dynamics*, M. Lesieur, P. Comte and J. Zinn-Justin (Ed.), Elsevier, New York, 67.
19. Donnelly, R. J., 1993, *Ann. Rev. Fluid Mech.*, 25, 325.
20. Zhou, H., 1997, *Phys. Fluids*, 9, 970.
21. Wang, H., 1998, *Phys. Rev. Lett.*, 80, 4665.